frontiers | Frontiers in Marine Science

TYPE Original Research
PUBLISHED 07 November 2023
DOI 10.3389/fmars.2023.1271638

OPEN ACCESS

EDITED BY
Ming Li,
University of Maryland, College Park,
United States

REVIEWED BY
Félix Margirier,
Alseamar, France
Manal Hamdeno,
University of Liège, Belgium
Arthur J. Miller,
University of California,
San Diego, United States

*CORRESPONDENCE
Elisabeth Kubin
kubin.elisabeth@gmail.com

RECEIVED 02 August 2023
ACCEPTED 18 October 2023
PUBLISHED 07 November 2023

CITATION
Kubin E, Menna M, Mauri E, Notarstefano G, Mieruch S and Poulain P-M (2023) Heat content and temperature trends in the Mediterranean Sea as derived from Argo float data. *Front. Mar. Sci.* 10:1271638. doi: 10.3389/fmars.2023.1271638

Heat content and temperature trends in the Mediterranean Sea as derived from Argo float data

Elisabeth Kubin[1]*, Milena Menna[1], Elena Mauri[1], Giulio Notarstefano[1], Sebastian Mieruch[2] and Pierre-Marie Poulain[1]

[1]Section of Oceanography, Institute of Oceanography and Applied Geophysics, Sgonico, Trieste, Italy, [2]Section of Marine Geology, Alfred Wegener Institute, Bremerhaven, Germany

The Mediterranean Sea is very sensitive to climatic changes due to its semi-enclosed nature and is therefore defined as one of the hotspots in future climate change projections. In this study, we use Argo float data to assess climatologies and trends in temperature and Ocean Heat Content (OHC) throughout the Mediterranean Sea and for specific sub-basins (e.g. Western and Eastern Mediterranean, Gulf of Lion, South Adriatic). The amount of the OHC, spatially averaged in bins of 1°x1° over the period from 2001 to 2020, increases from west to east in the Mediterranean Sea. Time series of temperature and OHC from 2005 to 2020, estimated in the surface and intermediate layers (5-700 m) and deeper layer (700-2000 m), reveal significant warming trends and an increase of OHC. The upper 700 m of the Mediterranean Sea show a temperature trend of 0.041 $\pm$ 0.012°C·yr^{-1}, corresponding to an annual increase in OHC of 3.59 $\pm$ 1.02 W·m^{-2}. The Western Mediterranean Sea (5-700 m) is warming fastest with an increase in temperature at a rate of 0.070 $\pm$ 0.015°C·yr^{-1}, corresponding to a yearly increase in OHC of 5.72 $\pm$ 1.28 W·m^{-2}. Mixing and convection events within convection sites and along boundary currents transport and disperse the temperature and OHC changes. Significant warming trends are evident in the deeper layers (700-2000 m) of the two deep convection sites in the Mediterranean Sea (Gulf of Lion, South Adriatic), with an exceptionally strong warming trend in the South Adriatic from 2013 to 2020 of 0.058 $\pm$ 0.005°C·yr^{-1}, corresponding to a yearly increase in OHC of 9.43 $\pm$ 0.85 W·m^{-2}. The warming of the different water masses will show its feedback on ocean dynamics and air-sea fluxes in the next years, decades, and even centuries as these warming waters spread or re-emerge. This will provide more energy to the atmosphere, resulting in more extreme weather events and will also stress ecosystems and accelerate the extinction of several marine species. This study contributes to a better understanding of climate change in the Mediterranean region, and should act as another wake-up call for policy makers and society.

KEYWORDS

heat content trends, temperature trends, Argo floats, Mediterranean Sea, Mediterranean sub-basins, dense water formation areas, climate change

1 Introduction

The Earth's climate is an open system, and the energy entering or leaving the Earth determines the Earth Energy Imbalance (EEI). The EEI is defined as the net radiative flux at the top of the atmosphere, i.e. as the difference between the incoming solar shortwave radiation and the outgoing infrared longwave radiation, and is considered the most fundamental metric for climate change. Anthropogenic greenhouse gas emissions caused a radiative imbalance at the top of the atmosphere that led to excessive heat within the Earth climate system (Trenberth and Stepaniak, 2004; von Schuckmann et al., 2016; Von Schuckmann et al., 2020; Trenberth et al., 2009; Hansen et al., 2011; Trenberth et al., 2014).

The World Ocean accounts for the uptake of 89% (90%) of the EEI over the period from 1971 to 2018 (2010-2018, respectively) in the upper 700 m (Levitus et al., 2012; Rhein et al., 2013; von Schuckmann et al., 2016; Von Schuckmann et al., 2020). The heat gain over land accounts for the uptake of 6% (5%) over these periods, while 4% (3%) go into the melting of grounded and floating ice and 1% (2%) go into atmospheric warming (Von Schuckmann et al., 2020). This quantification of the EEI – clearly shows that the ocean plays a major role in the heat uptake and storage. Therefore, the ocean heat content trend is a key component for the quantification of the EEI (Knutti and Rugenstein, 2015; Von Schuckmann et al., 2020; Cheng et al., 2023) and gives an estimate of the net climate forcing (Hansen et al., 2005; Levitus et al., 2005). It dominates the energy uptake with most of the warming absorbed by the upper layer (Rhein et al., 2013) and therefore acts as a strong buffer to climate change.

Due to the high heat capacity of seawater (Millero et al., 1973), small changes in seawater temperature lead to a large heat storage and therefore a strong increase in Ocean Heat Content (OHC). The global ocean warming for the period from 1955 to 2010 in the upper 700 m was found to be 0.18°C, corresponding to an increase in OHC of 0.27 Wm^{-2} (per unit area of the World Ocean; Levitus et al., 2012). The OHC is also directly linked to sea level rise through thermal expansion of the warmer waters, causing a thermosteric sea level rise of 0.41 $mmyr^{-1}$ for the upper 700 m layer of the World Ocean from 1955 to 2010 (Levitus et al., 2012; Church and White, 2011).

The region considered for our study is the Mediterranean Sea (MS), which is defined as one of the climate hotspots and plays an important role for climate change prediction (Giorgi, 2006; Bernstein et al., 2008; Lionello and Scarascia, 2018; Menna et al., 2022). Due to its reduced dimension, semi-enclosed morphology, and anti-estuarine circulation (evaporation exceeds over precipitation and river runoff), it responds faster to climatic changes than the global ocean (Giorgi, 2006; Schroeder et al., 2017). The MS occupies about 0.32% of the total volume of the global ocean, yet its unique geological history has resulted in high biodiversity with 7-10% of all known marine species (Bianchi and Morri, 2000; Coll et al., 2010). During the twentieth century it has undergone rapid changes with accelerating trends in temperature and salinity (Béthoux et al., 1998; Ozer et al., 2017; Schroeder et al., 2017) and climate model projections show a further acceleration in the future (Giorgi, 2006; Giorgi and Lionello, 2008; Kirtman et al., 2013). The MS is showing an increase not only in temperature and salinity, but also in sea level and freshwater fluxes during the period 1993-2020 (Menna et al., 2022). Many species are struggling to adapt to the rapidly warming waters, and more frequent marine heat waves are causing mass mortality events (Garrabou et al., 2022; Frölicher et al., 2018; Oliver et al., 2021; Smith et al., 2022).

Since the late 1980s, many studies have been conducted to quantify the trends of temperature and OHC in the MS (Vargas-Yáñez et al., 2008; Vargas-Yáñez et al., 2017; Iona et al., 2018). The time series of the averaged heat content anomaly from 1993 to 2019 (0- 700 m depth layer) shows a yearly trend of 1.4 ± 0.3 Wm^{-2} (OHC trend from Copernicus Marine Service; https://marine.copernicus.eu/access-data/ocean-monitoring-indicators). The yearly trend of temperature and sea level which was assessed from 1993 to 2021 is of 0.035 ± 0.002°C and 2.70 ± 0.83 mm, respectively (Copernicus Temperature and Sea Level Trend; https://marine.copernicus.eu/access-data/ocean-monitoring-indicators). The sea level rise is due to melting glaciers (Galassi and Spada, 2014; Marcos and Tsimplis, 2007; Lambeck and Bard, 2000) and thermal expansion (Criado-Aldeanueva et al., 2008; Tsimplis et al., 2008). In the surface layer, Pisano et al. (2020) found a yearly temperature trend of 0.041 ± 0.006°C for the whole MS from 1982 to 2018, using a satellite-based dataset. The trend shows uneven spatial patterns, with yearly trends of 0.036 ± 0.006°C and 0.048 ± 0.006°C for the Western Mediterranean and the Levantine-Aegean basin, respectively. In the period 1982-2020, Juza and Tintoré (2021) estimated trend values of 0.032 ± 0.002°Cyr^{-1} and 0.044 ± 0.002° Cyr^{-1} as averages in the Western and Eastern Mediterranean, respectively. Ibrahim et al. (2021) defined a trend of 0.033 ± 0.004°Cyr^{-1} in the Ionian Sea and Levantine basin. The rapid sea surface warming in the last two decades was associated with a strong increase in marine heatwave days (Bensoussan et al., 2019; Ibrahim et al., 2021; Juza and Tintoré 2021; Hamdeno and Alvera-Azcarate, 2023; Dayan et al., 2023).

The warming of the surface layer is transported toward deeper layers in the dense water formation areas of the MS: the Gulf of Lion (GoL; Grignon et al., 2010; Durrieu de Madron et al., 2013; Tamburini et al., 2013; Estournel et al., 2016; Conan et al., 2018), the Southern Adriatic Pit (SAP; Vilibić and Supić, 2005; Artegiani et al., 1989; Klein et al., 2000; Gačić et al., 2001; Manca et al., 2002; Cardin et al., 2011; Rubino et al., 2012; Janeković et al., 2014), the Aegean Sea and the Rhodes Gyre (Theocharis and Georgopoulos, 1993; Lascaratos et al., 1999; Malanotte-Rizzoli et al., 2003; Nittis et al., 2003; Theocharis et al., 2014; Roether et al., 2007; Kubin et al., 2019). Moreover, boundary currents also play an important role in transporting the changing water mass characteristics to deeper layers (Waldman et al., 2018; Kubin et al., 2019; Pinardi et al., 2019).

The trends of the MS can also influence the thermohaline cell of the North Atlantic (Potter and Béthoux, 2004; Béthoux et al., 1998; Rahmstorf, 1998). Through the Strait of Gibraltar, Mediterranean Intermediate Waters are exported to the Atlantic, therefore monitoring the temperature and OHC variations in the MS can contribute to the understanding of changes at global level.

This study aims to better understand the temperature changes and the heat storage in the MS. We used sub-surface temperature measurements by Argo floats, which is considered the most practical method to quantify the changes in temperature and OHC (Hansen et al., 2011; Von Schuckmann and Le Traon, 2011; von Schuckmann et al., 2016). We present the first climatology of OHC from *in situ* data in the MS (2001 to 2020). Trends of temperature and OHC for surface, intermediate, and deeper layers were calculated from 2005 to 2020 for the entire Mediterranean, as well as for specified sub-basins (Western and Eastern Mediterranean, the WWestMed, the WWestMed North, the WWestMedSouth and the deep dense water formation areas such as the Gulf of Lion and the South Adriatic Gyre; see Figure 1).

2 Dataset and methods

Argo floats are autonomous quasi-Lagrangian instruments that move with the ocean currents. They are considered expendable platforms but the small dimension of the MS offers a good chance of potential recoveries (Gonzalez-Santana et al., 2023). With the help of an external bladder, they modify their volume and are able to ascend and descend in the water column. They are programmed to be parked at a specific drifting depth (mostly at 350 or 1000 m) where they stay for a specified period (1-10 days, mostly 5 days in the MS; Poulain et al., 2007). Then, they descend to greater depths - up to 2000 m and 4000 m in the case of Core or Deep Argo floats. During their ascent back to the surface, they measure temperature and salinity (and eventually other biogeochemical parameters) throughout the water column (Wong et al., 2020). The typical vertical resolution of the profiles are 2 m (for 0-100 m), 10 m (for 100-700 m) and 25 m (for 700-2000 m). At the surface, Argo floats transmit the data to satellites and descend again to repeat their diving cycle.

Quality controlled Argo float data were downloaded from the Coriolis Global Data Assembly Center - GDAC (ftp://ftp.ifremer.fr/ifremer/argo/dac/coriolis; Cabanes et al., 2021; Argo float data and metadata from Global Data Assembly Centre (Argo GDAC), SEANOE, https://doi.org/10.17882/42182, 2020.). For this study, only data with the best quality control flags (qc=1, "good data") were considered for each float profile and, to additionally ensure the correctness of the data, a visual inspection of all the temperature profiles was performed. The quality controlled data were subsampled over time intervals of 5 days in order to obtain a homogenous data set, i.e. one Argo float profile every 5 day interval.

The total number of Argo float profiles subsampled every 5 days exceeds 38.000 (Figure 2A). The temporal and geographical distribution of these profiles show a strong increase starting in 2012. The geographical distribution (Western and Eastern Mediterranean) is similar for the different seasons (Figure 2B).

There are different methods to derive the OHC: it can be inferred by the surface heat flux from space, the thermal expansion of the sea (thermosteric sea level rise) from space or directly by using *in situ* temperature profiles. These subsurface temperature measurements are the most practical way to quantify the excess heat (Kirtman et al., 2013). In this study, we therefore use the available Argo float data to assess the climatology and the warming trends of temperature and OHC in the MS. For the OHC computation, different formulas were tested (Equation 1-3; ϱ_z : depth dependent density; C_p : specific heat capacity; θ : potential temperature; S: salinity; T: temperature) and the results were found to be consistent with one another.

$$\langle OHC \rangle = \varrho_z \cdot C_p \cdot \langle \theta \rangle \cdot \Delta z \qquad (Jorda\ et\ al.,\ 2017) \qquad 1)$$

$$\langle OHC \rangle = \varrho_z \cdot C_p(\theta, S) \cdot \langle \theta \rangle \cdot \Delta z \qquad (Artale\ et\ al.,\ 2017) \qquad 2)$$

$$\langle OHC \rangle = \varrho_0 \cdot C_p \cdot \langle T \rangle \cdot \Delta z \quad (Von\ Schuckmann\ et\ al.,\ 2018) \quad 3)$$

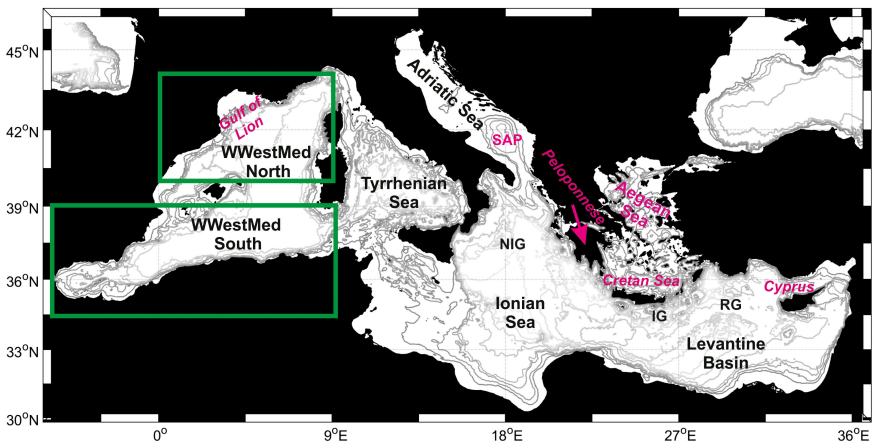

FIGURE 1
Bathymetric map (isobaths every 500 m) of the Mediterranean Sea, its sub- and sub-sub-basins and dense water formation sites mentioned in this work. Sub-basins: Western Mediterranean< 15°E; Eastern Mediterranean > 15°E; Sub-sub-basins: WWestMed, the western part of the Western Mediterranean Sea< 9°E; WWestMedNorth, the northern part of the WWestMed; WWestMed South, the southern part of the WWestMed (see green rectangles); SAP, the South Adriatic Pit; NIG, the North Ionian Gyre; IG, the Iera Petra Gyre and RG, the Rhodes Gyre. For exact coordinates see Table 1.

TABLE 1 Mean temperature and standard deviation and temperature and OHC trends and associated error from 2005 to 2020 for surface and intermediate (5-700 m) and deeper (700-2000 m) layers.

	Surface + Intermediate Layers (5 – 700 m)				Deep Layers (700 – 2000 m)			
	Mean Temp ± std	ΔT [°Cyr^{-1}]	ΔOHC [Wm^{-2}yr^{-1}]	Data-points	Mean Temp ± std	ΔT [°Cyr^{-1}]	ΔOHC [Wm^{-2}yr^{-1}]	Data-points
Med 30 – 46°N -6 – 38°E	15.4±1.3	0.041±0.012	3.59 ± 1.02	41293	13.6 ± 0.4	*0.001 ± 0.008*	*0.15 ±1.25*	25999
WestMed 34 – 44°N -6 – 15°E	14.6 ±1.0	0.070 ± 0.015	5.72 ± 1.28	18486	13.3 ± 0.3	*0.000 ± 0.010*	*-0.04 ±1.75*	11645
EastMed 30 – 46°N 15 – 38°E	16.0 ±1.3	*0.025 ± 0.024*	*2.18 ±2.19*	22807	13. ± 0.3	*-0.005 ±0.003*	*-0.74 ±0.47*	14354
WWestMed 34 – 44°N -6 – 9°E	14.4 ± 1.0	0.063 ± 0.014	5.46 ± 1.21	13419	13.2 ± 0.1	*0.004 ± 0.005*	*0.71 ± 0.71*	9396
WWestMed North 40 – 44°N 0 – 9°E	14.1 ± 0.8	0.068 ± 0.015	5.67 ± 1.32	5878	13.2 ± 0.1	0.006 ± 0.002	1.03 ± 0.38	4489
WWestMed South 34 – 39°N -6 – 9°E	14.7 ± 0.9	0.074 ± 0.007	6.47 ± 0.10	5578	13. ± 0.1	*0.001 ± 0.004*	*0.19 ± 0.57*	3584
Gulf of Lion (From 2005) 41.5 – 43.65° N 3 – 6.2°E	14.0 ± 0.6	0.046 ± 0.021	4.00 ± 1.81	1232	13.2 ± 0.1	0.008 ± 0.003	1.22 ± 0.44	979
Gulf of Lion (From 2013) 41.5 – 43.65° N 3 – 6.2°E	13.5 ± 0.2	0.044 ± 0.015	3.02 ± 1.02	914	13.2 ± 0.1	0.017 ± 0.003	2.70 ± 0.47	713
South Adriatic (From 2013) 41.5 – 42.5°N 17 – 18.5°E	15.0 ± 0.5	*- 0.021 ± 0.023*	*- 1.84 ± 1.97*	991	13. 7± 0.2	0.058 ± 0.005	9.43 ± 0.85	571

Trends are considered significant if they are twice as large as the associated error (95% confidence interval). Non significant values are in red.

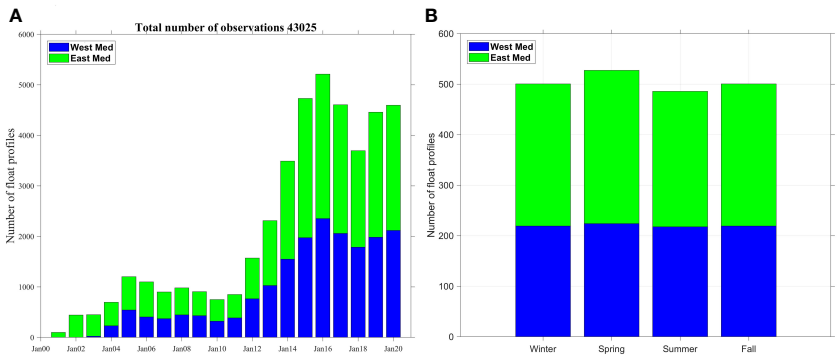

FIGURE 2
(A) Number of Argo float profiles per year within the Mediterranean divided in Western (blue bars) and Eastern (green bars) basins. **(B)** Number of Argo float profiles for the Western and the Eastern Mediterranean basins for winter (JFM), spring (AMJ), summer (JAS) and autumn (OND) from 2001 to 2020.

For this study, we have chosen Equation 3, which has been used for recent estimates of OHC for the global ocean as well as for the MS (both for a depth range of 0-700 m and a time range from 2005 to 2019 and 1993 to 2019, respectively; https://marine.copernicus.eu/access-data/ocean-monitoring-indicators?category=105&region=all&search). The mean OHC per Argo float profile $\langle OHC \rangle$ is proportional to the mean temperature $\langle T \rangle$ within a certain depth interval $\Delta z = z2 - z1$, with a reference density of $\varrho_{0\ =}$ 1030 kgm^{-3} and a specific heat capacity of C_p=3980 $Jkg^{-1}°C^{-1}$ (Von Schuckmann et al., 2009). Units of OHC are Jm^{-2}.

Float profiles available in the period 2001-2020 were organized in bins of 1°x1°. The climatologies of the $\langle OHC \rangle$ were estimated for each bin within different vertical layers (different Δz) : the whole layer measured by the Argo floats (5-2000 m), the surface and intermediate layers considered together (5-700 m), the surface (5-150 m), intermediate (150-700 m) and deep (700-2000 m) layers separately. The OHC distribution in the deepest part of the MS is not yet reported in the literature, so the deepest layer measured by floats (1500-2000 m) was also considered for the climatologies.

The trends of temperature and OHC were estimated in the period from 2005 to 2020, due to a limited number of float profiles available before 2005. For the trend calculation, we considered surface and intermediate layers together (5-700 m), the deeper layer (700-2000 m) and surface (5-150 m) and intermediate (150-700 m) layers separately.

Trends were computed using a linear least squares method combined with an autocorrelation correction, following Mieruch et al. (2008) and Weatherhead et al. (1998). The reason for using such a correction is that environmental data are typically autocorrelated. Thus the typical assumption of uncorrelated (white noise) fit residuals in estimating linear trends cannot be justified, and would yield to an underestimation of the trend uncertainties, the errors. Our trend analysis and the interpretation is based on annual data, therefore we can use the simple trend model:

$$Y_t = \mu + \omega X_t + N_t, \quad 4)$$

where Y_t are the annual parameters (e.g. temperature), μ is the ordinate, ω represents the trend, X_t is the time (years) and N_t is the autocorrelated noise and modelled as an autoregressive process of order 1 (AR[1]):

$$N_t = \phi N_{t-1} + \epsilon_t, \quad 5)$$

where φ is the autocorrelation at lag one (-1<φ<1) and ϵ_t is considered as the independent non-correlated noise component. For the details of the estimation of the trend and its error we refer to Mieruch et al. (2008). Finally, according to probability theory, an estimated trend ω is considered statistically significant with a probability of 95% if it is twice as large as its error:

$$|\omega| \geq 2\sigma_\omega, \quad 6)$$

The trend analysis of temperature and OHC was done for the whole Mediterranean Sea as well as for specified sub-basins and was expressed in °C per year [°C·yr^{-1}] and Watt per square metre [W·m^{-2}] per year, respectively.

3 Results

3.1 Climatologies and distribution of OHC

The spatial distribution of the number of observations derived by Argo floats in bins of 1°x1° decreased with the increasing layer depth in the period 2001-2020 (Figure 3). For the depth interval of 5-700 m a maximum number of 600 Argo floats profiles per bin was reached within the area of the SAP, followed by 400 and 500 profiles within the area of the Gulf of Lion and the Ierapetra Gyre (IG), respectively (Figures 3A, B). In the deep layer (Figure 3C), maxima of 350 profiles were observed within the areas of the Northwestern Mediterranean, the SAP and the IG.

The mean OHC was estimated in different layers, along with the related standard deviations, and showed values of different magnitude for the respective layers due to the strong influence of Δz on the OHC (see Equation 3). Therefore, a specific colour bar was used for each depth layer. Moreover, to make the different layers comparable, the amount of OHC per 100 m was also listed for each layer (Figures 4, 5; Table 2).

The amount of the OHC increased moving from west to east in the MS within all layers (Figures 4, 5, left panel). The total amount of the mean OHC over the entire water column measured by the Argo floats (5-2000 m) can be seen in Figure 5A, left panel. Approximately 38% of this heat was stored in the 5-700 m layer (Figure 4A; Table 2), ~ 9% was stored in the surface (5-150 m; Figure 4B; left panel; Table 2) and ~ 28% in the intermediate (150-700 m; Figure 4C, left panel; Table 2) layers. The deep layer (700-2000 m; Figure 5B, left panel; Table 2) stored ~63% of the heat. A focus on the deepest part of the MS sampled by floats (1500-2000 m) showed a heat amount of ~ 24% of the total, with largest values in the Cretan Sea (Figure 5C, left).

The standard deviations were at least one order of magnitude smaller than the estimated means (Figures 4-5; Table 2). Considering the three layers separately, the highest range of variability of the OHC per 100 m was observed in the surface layer (7 10^8 Jm^{-2}), followed by the intermediate (5 10^8 J m^{-2}) and finally by the deep layer (4 10^8 Jm^{-2}).

The surface layer showed the expected low amount of OHC within dense water formation sites such as the Gulf of Lion, the South Adriatic Gyre (SAP), the Aegean Sea and the Rhodes Gyre (Figure 4B). Larger values of the OHC were observed in the in the Cretan Sea, in the Peloponnese area and south of Cyprus in the surface layer (5-150 m; Figure 4B, left), along the southern and eastern coasts of the Levantine Basin in the intermediate layer (150-700 m; Figure 4C, left), in the Cretan and southern Aegean seas in the deep layer (700-2000 m; Figure 5B, left). The Ionian Sea acted as a "transition basin" between the lower OHC values of the Western Basin and the larger values of the Levantine Basin. The Tyrrhenian and the Adriatic seas showed values comparable with the Western Basin (Figure 4B). In the intermediate and deep layers, it was rather the Tyrrhenian and the Southern Adriatic basins that held OHC values intermediate between the westernmost and the easternmost part of the Mediterranean (Figures 4C, 5B; left).

10.3389/fmars.2023.1271638

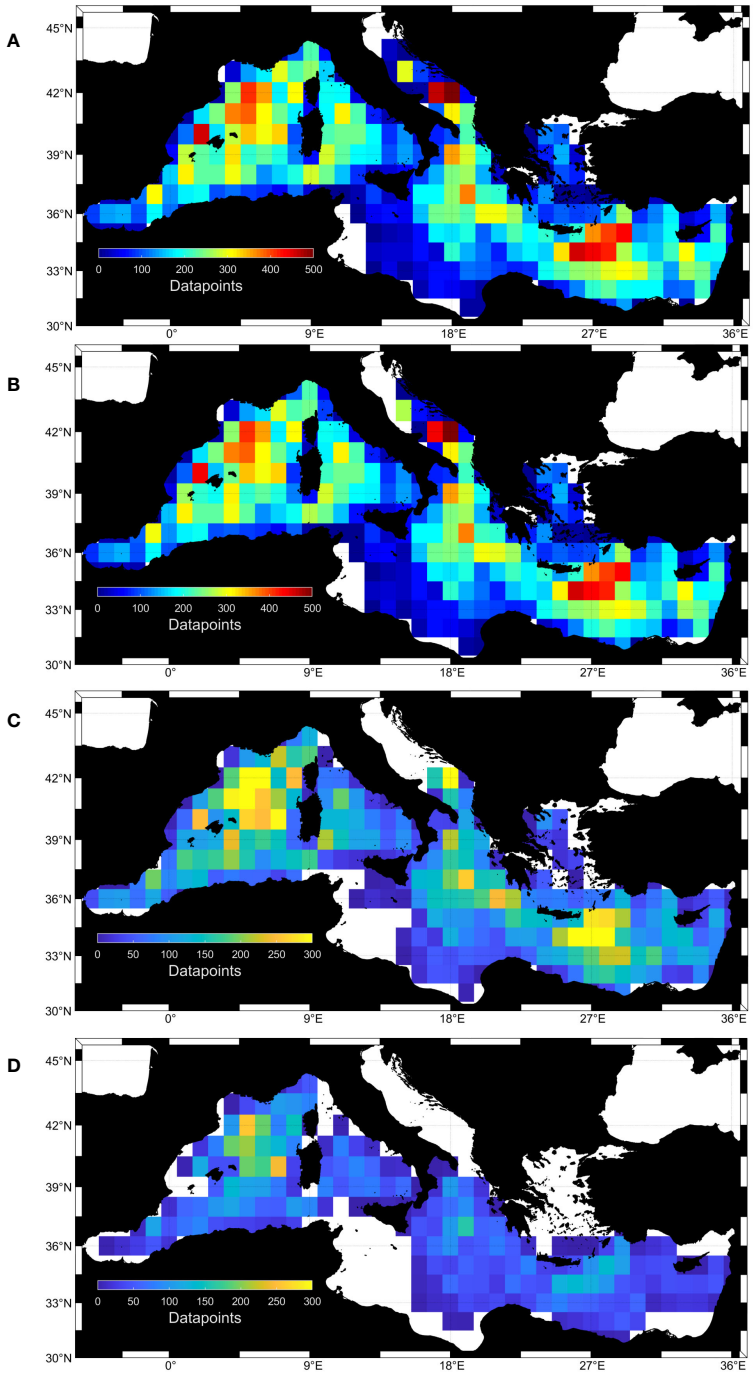

FIGURE 3
Number of float profiles from 2001 to 2020 within 1°x1° grid boxes for **(A)** the surface layer (5-150 m); **(B)** the intermediate layer (150-700 m); **(C)** the deeper layer (700-2000 m) and **(D)** the deepest layer (1500-2000 m) measured by the Argo floats.

The deepest layer measured by the Argo floats (1500 – 2000 m; Figure 5C) revealed four main different sub-basins in the OHC distribution, confirming the increase in OHC from west to east: the western part of the Western Mediterranean (6°W< longitude< 9°E; OHC values smaller than 26.5 10^{10} Jm^{-2}), the Tyrrhenian Sea (9°E< longitude< 16°E; OHC values range from 26.5 10^{9} to 26.7 10^{9} Jm^{-2}), the Ionian Sea (16°E< longitude< 23°E; OHC values range from 27 10^{9} to 27.7 10^{9} Jm^{-2}) and the Levantine with the Cretan Sea (25°E< longitude< 38°E; OHC values range from 27.25 10^{9} to 28.5 10^{9} Jm^{-2}).

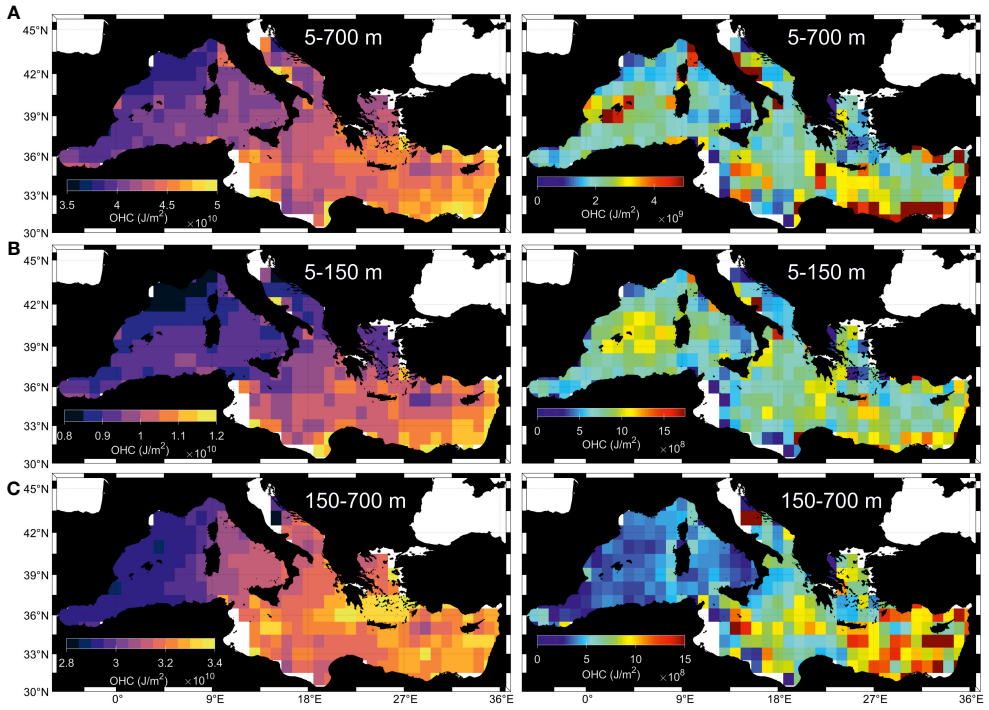

FIGURE 4
Left panel: Mean OHC from 2001 to 2020 within 1°x1° grid boxes for **(A)** the surface and intermediate layers together (5 - 700 m), **(B)** the surface layer (5-150 m) and **(C)** the intermediate layer (150-700 m). Right Panel: Standard deviation around the mean OHC. Please note the different colour scales.

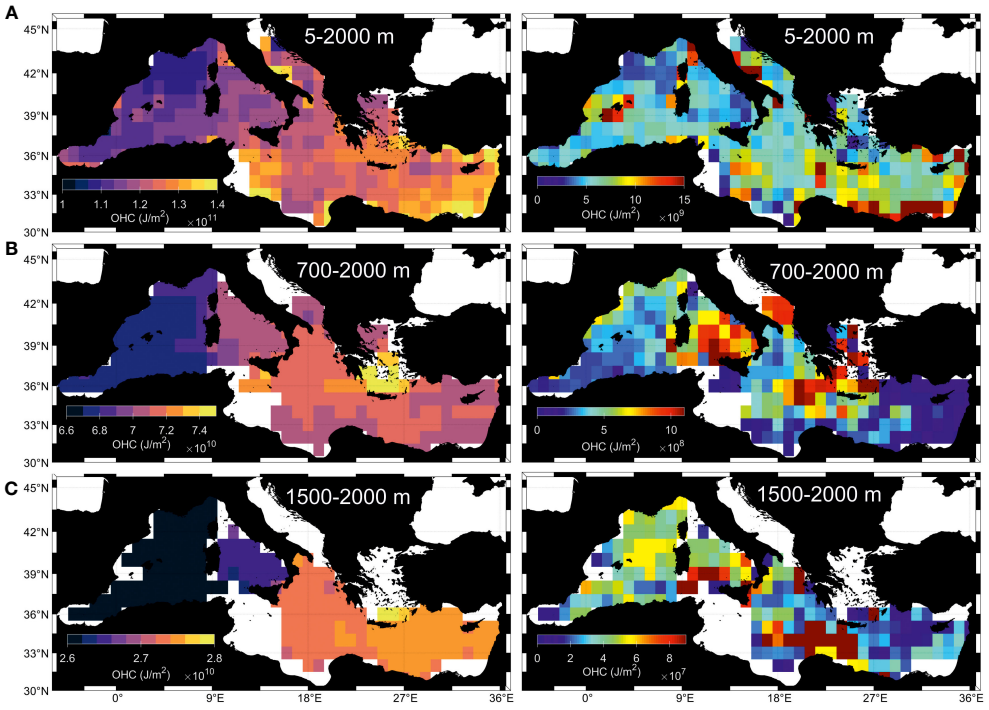

FIGURE 5
Left panel: Mean OHC from 2001 to 2020 within 1°x1° grid boxes for **(A)** the entire depth layer (5-2000 m), **(B)** the deeper layers (700-2000 m) and **c)** the deepest layers (1500-2000 m) measured by Argo floats. Right Panel: Standard deviation around the mean OHC. Please note the different colour scales.

10.3389/fmars.2023.1271638

TABLE 2 Mean OHC and relative standard deviation for all the layers considered (see Figures 4 and 5) derived for the whole depth layer Δz and per 100 m.

	Mean OHC for Δz	Std mean OHC for Δz	Mean OHC per 100 m	Std mean OHC per 100m	Nr of bins
5–700 m	409	41	59	6	337
5–2000 m	1160	114	58	6	337
5–150 m	92	10	64	7	337
150–700 m	300	27	54	5	332
700–2000 m	673	50	52	4	295
1500–2000 m	258	20	52	4	222

The values retrieved for the surface, intermediate, and deep layers are highlighted in yellow. Units are in 10^8 J·m^{-2}.

3.2 Trends of temperature and OHC

The trends of temperature and OHC were analyzed for surface and intermediate layers together (5-700 m; Table 1), for deep layers (700-2000 m; Table 1) and for surface and intermediate layers separately (Table 3). The respective trends were calculated from annual averaged data and are shown in Tables 1 and 3. Monthly averaged temperatures for the entire MS, the Western and the Eastern basins considering the surface and intermediate layers together (5-700 m) are shown in Figure 6.

In the first 700 m of the water column, the warming rate was of 0.041 ± 0.012°C·yr^{-1} (Figure 6; Table 1). This positive trend was larger in the Western Mediterranean, which showed an increment of temperature of 0.070 ± 0.015°C·yr^{-1} (Figure 6; Table 1). The Eastern Mediterranean displayed a weaker positive trend with a temperature increase of 0.025 ± 0.024°C·yr^{-1} (Figure 6; Table 1). The latter trend is not significant due to the high error (see Methods for trend and error calculation). The temperature in the deep layers of the Western, Eastern and the entire MS exhibited no significant trends during the period considered (Table 1).

The Southwestern part of the Western Mediterranean (WWestMedSouth; Table 1) showed the strongest sub-basin warming rate in the layer 5-700 m (0.074 ± 0.007°C.yr^{-1}) within the entire MS. The WWestMedNorth (Table 1), that includes the deep dense water formation site Gulf of Lion, described a significant and strong warming rate in the layer 5-700 m and in the deep layer of 0.068 ± 0.015°C·yr^{-1} and of 0.006 ± 0.002°C·yr^{-1}, respectively (Table 1). The annual increase in OHC in the intermediate and deep layers correspond to 5.14 ± 1.31 W·m^{-2} and 1.20 ± 0.36 W·m^{-2}, respectively.

Significant warming trends within the surface and the intermediate layers considered separately were observed for the entire MS as well as for the Western Mediterranean, while the Eastern Mediterranean did not show statistically significant trends within these layers (Table 3). For surface and intermediate waters, the Eastern Mediterranean showed the highest mean temperature and the highest sub-basin standard deviation of 17.6 ± 1.9°C and 14.8 ± 0.6°C. The strongest warming of surface and intermediate waters occurred in the Western Mediterranean, with a temperature increase of 0.090 ± 0.017°C·yr^{-1} and 0.030 ± 0.008°C·yr^{-1}, respectively. The deep dense water formation site Gulf of Lion showed significant warming trends in all layers from 2005 to 2020 (Table 1; Table 3).

A detailed analysis of temperature trends in the two main convection areas of the MS, the Gulf of Lion and the SAP, showed strong warming in these areas. Trends in the Gulf of Lion were estimated both from 2005, including all available float profiles, and from 2013 to be comparable with the time series of the SAP, where data are available from a more recent period (see Figure 7 and Tables 1, 3). In the Gulf of Lion, the two trends (since 2005 and since 2013) were very similar in the first 700 m of the water column (Table 1); in contrast, a double warming was observed in the intermediate (Table 3; Figure 7A, left panel) and deep (Table 1; Figure 7B, left panel) layers since 2013, suggesting that the warming from 2013 occurred at a faster rate than before.

In the SAP, surface and intermediate layers showed not statistically significant trends while the deep layer exhibited a significant warming of 0.058 ± 0.005°C·yr^{-1} (Figure 7B, right panel; Table 1; annual increase of 9.43 ± 0.85 W·m^{-2}). The rate of warming of the deep layer in the Gulf of Lion since 2013 (0.017 ± 0.003°C·yr^{-1}; annual increase of 2.70 ± 0.47 W·m^{-2}) is less than a third of the SAP (0.058 ± 0.005°C·yr^{-1}; Figure 7B; Table 1; annual increase of 9.43 ± 0.85 W·m^{-2}).

4 Discussion and conclusions

This work adds new insights on the OHC distribution and variability in different depth layers of the MS, focusing on the differences among the sub-basins and on the behavior of deep dense water convection sites. The 1°x1° climatologies from 2001 to 2020 show an increase in OHC from west to east (Figures 4, 5). The dense water formation sites such as the Gulf of Lion, the SAP, the Aegean Sea and the Rhodes Gyre show the expected low amount of OHC (Figure 4A). Surface layers (5-150 m; Figure 4B) show a high amount of OHC along the boundary currents within the Levantine Sea. Intermediate layers (150-700 m; Figure 4C) also exhibit a high amount of OHC within the Levantine, the Aegean and within parts of the Ionian Sea. The deepest layer measured by the Argo floats (1500-2000 m; Figure 5C) reveals four main different

TABLE 3 Mean temperature and standard deviation and temperature and OHC trends and associated error from 2005 to 2020 for surface (5-150 m) and intermediate (150-700 m) layers.

	Surface Layers (5 – 150 m)				Intermediate Layers (150 – 700 m)			
	Mean Temp ± std	ΔT [°Cyr^{-1}]	ΔOHC [Wm^{-2}yr^{-1}]	Data-points	Mean Temp ± std	ΔT [°Cyr^{-1}]	ΔOHC [Wm^{-2}yr^{-1}]	Data-points
Med 30 – 46°N -6 – 38°E	16.8 ± 2.0	0.035 ± 0.015	0.64 ± 0.27	41225	14. 3± 0.7	0.019 ± 0.007	1.34 ± 0.48	40242
WestMed 30 – 46°N -6 – 15°E	15.7 ± 1.6	0.090 ± 0.017	1.64 ± 0.31	18476	13. 7± 0.4	0.030 ± 0.008	2.10 ± 0.55	17854
EastMed 30 – 46°N 15 – 38°E	17.6 ±1.9	*0.002 ±0.025*	*0.034 ±0.45*	22749	14. 8±0.5	*0.015 ±0.016*	*1.04 ±1.10*	22388
Gulf of Lion (From 2005) 41.5 – 43.65° N 3 – 6.2°E	14.6 ± 1.2	0.067 ± 0.025	1.21 ± 0.46	1232	13.4 ± 0.2	0.023 ± 0.006	1.61 ± 0.41	1228
Gulf of Lion (From 2013) 41.5 – 43.65° N 3 – 6.2°E	14.8 ± 1.3	*0.015 ± 0.090*	*0.27 ± 1.63*	918	13.4 ± 0.2	0.044 ± 0.015	3.02 ± 1.02	914
South Adriatic (From2013) 41.5 – 42.5°N 17 – 18.5°E	15.7 ± 0.9	*-0.047 ± 0.032*	*- 0.84 ± 0.58*	991	14. 3± 0.2	*0.027 ± 0.019*	*1.88 ± 1.33*	990

Trends are considered significant if they are twice as large as the associated error (95% confidence interval). Not significant values are in red.

sub-basins regarding the OHC distribution, with an increase in OHC from west to east: the West Western Mediterranean, the Tyrrhenian Sea, the Ionian Sea and the Levantine Sea.

Time series of temperature and OHC from 2005 to 2020 revealed significant positive trends in the upper 700 m of the water column, of 0.041± 0.012°C·yr^{-1} and of 3.59 ± 1.02 W·m^{-2}·yr^{-1}, respectively (Figure 6; Table 1).

Compared to the annual OHC trend of 1.5 ± 1.02 Wm^{-2}, estimated in the period from 1993 to 2018 by Von Schuckmann et al. (2018; see Equation 3 and for dataset description: https://

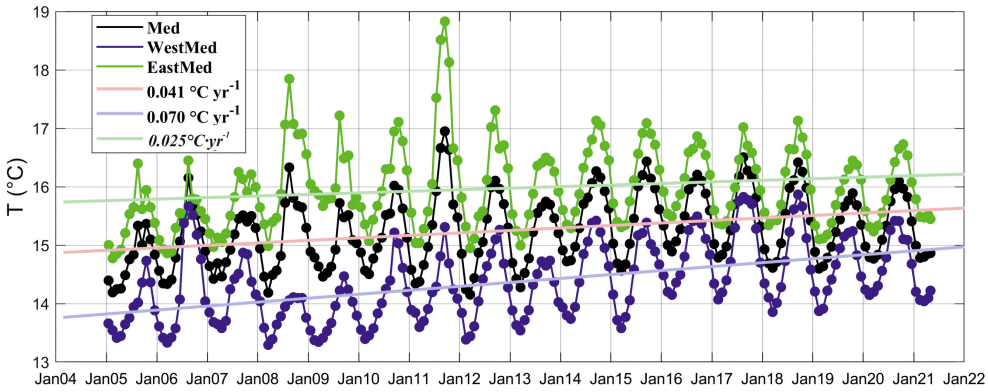

FIGURE 6
Time series of monthly mean temperature and calculated trends of annual mean temperature [°C] for surface and intermediate layers (5-700 m). Black, blue and green points indicate monthly mean temperatures within the entire Mediterranean Sea, the Western (longitude<15°) and the Eastern (longitude>15°) Mediterranean Sea, respectively. For the specified depth intervals the magenta, green and blue lines show the best linear fit and trend for the entire Mediterranean Sea and the Eastern and Western Mediterranean Sea, respectively. The trend is only significant (95th percentile) if it is twice as large as the error; statistically not significant trends are written in cursive.

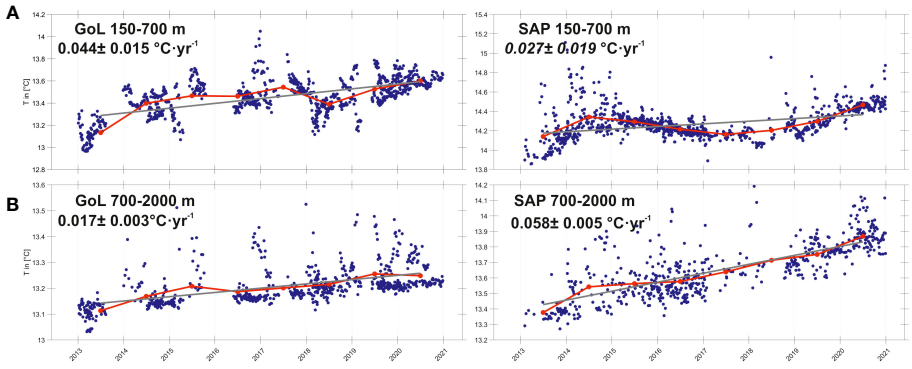

FIGURE 7
Trend of temperature from 2013 to 2020. Left panel: Gulf of Lion (GoL). Right panel: the South Adriatic Pit (SAP) for **(A)** intermediate (150-700 m) and **(B)** deep (700-2000 m) layers (see Tables 1, 3 for values and coordinates). The text box shows the yearly temperature trend; statistically not significant trends are written in cursive. The red curve shows the annual mean temperatures.

marine.copernicus.eu/access-data/ocean-monitoring-indicators?category=105&region=all&search), the annual trend derived from Argo float data in the period 2005 - 2020 appears more than doubled. Although this result comes out from two different datasets, it clearly indicates a significant increase of the heat accumulation rate over the last 15 years.

The upper 700 m of the Western Mediterranean are warming fastest with an increase in temperature of 0.070± 0.015°C·yr^{-1}, corresponding to an increase in OHC of 5.72 ± 1.28 W·m^{-2}·yr^{-1} (Table 1). These results pave the way for a new "view" of Mediterranean warming trends than those derived from SST-based estimations (Pisano et al., 2020; Juza and Tintore, 2021), which defined an uneven spatial pattern with increasing trends going from west to east. However, according to the float dataset, the Western basin holds less heat (lower OHC in Figure 4) than the Eastern basin (higher OHC in Figure 4), but with a steep warming trend (Tables 1, 3).

The southern part of the Western Mediterranean Sea (WWestMed South in Figure 1) exhibits the strongest sub-sub-basin warming trend of the MS for the upper 700 m, which is related to the warming of the resident Mediterranean Intermediate Water (MIW). The MIW is a water mass composed of a mixture of waters coming from the Eastern basin: the Levantine Intermediate (LIW) and the Cretan Intermediate Water (CIW, https://ciesm.org/MWM_Acronyms/MedWaterMassAcronyms.pdf). The heat gain in the MIW (0.019 ± 0.007°Cyr^{-1}, see Table 3) and in particular in the Western Intermediate Water (WIW, https://ciesm.org/MWM_Acronyms/MedWaterMassAcronyms.pdf) of 0.019 ± 0.007°Cyr^{-1} also provides information about the warming of the Mediterranean Outflow Waters (MOW), the saline and warm water mass located in the intermediate depths of the North Atlantic and produced by the outflow of Mediterranean water through the Strait of Gibraltar (Millot et al., 2006; Naranjo et al., 2015; de Pascual-Collar et al., 2019). This water mass is one of the most important intermediate water masses in the North Atlantic; it is involved in the North Atlantic Deep Water formation processes and its properties and variability have a significant impact on global climate (Aldama-Campino and Döös, 2020).

Significant warming trends are evident in the intermediate and deep layers (Figure 7) of the two deep convection sites in the MS (Gulf of Lion, South Adriatic; Figure 1), with an exceptionally strong warming trend in the South Adriatic in 2013-2020 (Figure 7B, right panel; Table 1). This result is consistent with recent studies showing a steady temperature increase in the deep layer of this area (Civitarese et al., 2005; Cardin et al., 2011; Cardin et al., 2020). Thermohaline properties in the SAP are closely related to the periodic reversal (from anticyclonic to cyclonic and vice-versa) of the Northern Ionian Gyre (NIG; Gačić et al., 2010; Menna et al., 2019; Rubino et al., 2020; Gačić et al., 2021) on a quasi-decadal temporal scale (Civitarese et al., 2010; Mihanović et al., 2021). NIG reversals affect the water mass distribution among the Eastern Mediterranean sub-basins (Gačić et al., 2011; Bessières et al., 2013; Reale et al., 2017; von Schuckmann et al., 2019), in turn influencing the thermohaline properties of the whole Mediterranean on decadal and multi-decadal scales (Gačić et al., 2013; Schroeder et al., 2017; Placenti et al., 2022). The effect of the NIG reversal on the SAP intermediate layer results in a clear oscillation in the temperature time series (Figure 7A, right panel). Larger values are observed during the cyclonic phase (2014-2015 and 2020-2021), which favors the inflow in the SAP of water of Levantine origin (warmer and saltier), and lower values during the anticyclonic phase, which favors the inflow of water of Atlantic origin (colder and less salty). Although less pronounced, a temperature oscillation is also observed in the deep layer that is in phase with that of the intermediate layer, emphasizing the role of convective mixing and winter convection in the vertical distribution of properties and associated long-term variations in the water column.

The Gulf of Lion also shows quasi-decadal variations in the intermediate layer (Figure 7A, left panel), which are probably also related to the LIW temperature variations associated with the NIG reversals. Gačić et al. (2013) defined a travel time of the LIW between the Sicily Channel and the Gulf of Lion of ~ 10-12 yr, while Placenti et al. (2022) found a lag of ~ 9-10 yr between the NIG reversals and their effect in the Sicily Channel. Combining these two results, it can be argued that the temperature increase (decrease) in the intermediate layer of the Gulf of Lion (Figure 7A, left panel) in 2014-2017 (2018-2019) can be related to the temperature increase (decrease) observed in the Sicily Channel in 1998-2006 (2007-2010), which in turn is related to

the anticyclonic (cyclonic) NIG of 1988-1996 (1998-2005) (see Figure 6 in Placenti et al., 2022). Quasi-decadal temperature fluctuations in the deep layer in the Gulf of Lion (Figure 7B, right panel) appear to be out of phase with the intermediate layer (Figure 7A, right panel), revealing a weak communication between the two layers. This result can be a consequence of the absence of bottom-reaching convection in the Western Mediterranean since 2014 (Josey and Schroeder, 2013; Margirier et al., 2020). Under these conditions, the intermediate waters in the Gulf of Lion became warmer and saltier throughout the basin (Margirier et al., 2020), supporting the steep trend observed in Figure 7A (left panel) compared to the previous period (Table 3).

The advection and diffusion of the temperature and the OHC leads to a general warming of the deeper sea. The sinking of surface water masses does not only take place within the deep dense water formation sites, but also along boundary currents. This has been shown by theoretical (Waldman et al., 2018; Pinardi et al., 2019) and experimental (Kubin et al., 2019) studies within the MS: the net sinking along the boundary currents is due to the conservation of potential vorticity and serves to balance the friction along the boundary currents. As a consequence, the warming of deeper layers might be more intense than previously thought and can potentially shift deeper ecosystems within the deep dense water formation sites (Tamburini et al., 2013; Coma et al., 2009).

In fact, the high amount of OHC in the surface layer along the boundary currents in the Levantine Sea (Figure 4B) is transported to intermediate (and eventually also to deeper) layers. The warm Levantine Intermediate Water (LIW) enters the Aegean Sea through the Cretan Straits as Modified Levantine Intermediate Water (MLIW; Velaoras and Lascaratos, 2010), leading to warm Aegean intermediate waters and as a consequence also to warm intermediate waters exhibiting a high amount of OHC within the Ionian Sea (outflow of the Aegean Sea; Figure 4C).

The warming of these surface and intermediate water masses also influences the preconditioning for the deep convection site in the Gulf of Lion (Grignon et al., 2010; Estournel et al., 2016).

The subduction and spreading of surface water anomalies and the consequent warming of intermediate and deep water masses are already showing their feedback on ocean dynamics and the atmosphere (air-sea fluxes) and will continue to do so in the coming years, decades, or even centuries as these warming water masses spread or re-emerge (Artale et al., 2018; Lo Bue et al., 2021). Marine heatwaves have also become and will become more frequent (Frölicher et al., 2018; Darmaraki et al., 2019a; Darmaraki et al., 2019b; Oliver et al., 2021; Juza et al., 2022; Hamdeno and Alvera-Azcarate, 2023). These unprecedented changes will stress ecosystems and accelerate the loss of biodiversity and the extinction of several marine species who cannot adapt to such rapid temperature changes (Garrabou et al., 2022; Smith et al., 2022; Fragkopoulou et al., 2023). Moreover, impacts of climate change also threaten indigenous cultures and their knowledge about the ocean and ecosystems (Bindoff et al., 2019).

Therefore, this study should act as another wake up call for policy makers and society. The stabilization of the climate - agreed by the UNFCCC in 1992 and the Paris agreement in 2015 - would require that the EEI is reduced to approximately zero in order to achieve the Earth's system quasi-equilibrium, which corresponds to a decrease of atmospheric CO_2 from 410 ppm to 353 ppm (Von Schuckmann et al., 2020). This can only happen if social, economic and ecological development are no longer seen as separate parts, but as interconnected (Berkes, 2017; Von Schuckmann et al., 2020).

The 2021-2030 UN Decade of Ocean Science for Sustainable Development aims to create a more holistic and integrated approach, with an emphasis also on indigenous people and the traditional knowledge of local people to achieve a truly sustainable approach and not just green- or bluewashing projects. Blue economy and blue growth is often doing more harm than good, because it is still based on exploitation and on the concept of economic growth on a finite planet (Ehlers, 2016), while indigenous people and their traditional conservation and management are based on the respect of nature and taking care of the land (Minerbi, 1999; Kealiikanakaoleohaililani and Giardina, 2016; Berkes, 2017; Witte and Xué, 2018; UNESCO Man and Biosphere Programme, Reed, 2019). Such holistic ways of understanding the environment offer alternatives to the prevailing consumption-oriented values of Western societies (Berkes and Turner, 2006; Kimmerer, 2012; Brondízio et al., 2021).

Therefore, possible solutions cannot only be of technological nature, but require an urgent and strong shift of our way of thinking and of our entire worldview to make sure that future generations can experience healthy, living oceans and ecosystems.

Data availability statement

Publicly available datasets were analyzed in this study. This data can be found here: Argo float data and metadata from Global Data Assembly Centre (Argo GDAC), SEANOE, https://doi.org/10.17882/42182, 2020.

Author contributions

EK: Conceptualization, Data curation, Investigation, Methodology, Writing – original draft, Writing – review & editing, Software, Visualization. MM: Funding acquisition, Investigation, Visualization, Writing – original draft, Writing – review & editing. EM: Funding acquisition, Writing – review & editing. GN: Data curation, Writing – review & editing. SM: Investigation, Software, Writing – original draft, Writing – review & editing. PP: Conceptualization, Funding acquisition, Methodology, Writing – review & editing.

Funding

The author(s) declare financial support was received for the research, authorship, and/or publication of this article. This research was funded by the Italian Ministry of University and Research as part of the Argo-Italy program.

Acknowledgments

We thank all the people involved with the preparation and deployment of the Argo floats in the Mediterranean Sea. In particular, special thanks to Antonio Bussani and Massimo Pacciaroni for the help with the data processing.

Conflict of interest

The authors declare that the research was conducted in the absence of any commercial or financial relationships that could be construed as a potential conflict of interest.

Publisher's note

References

Aldama-Campino, A., and Döös, K. (2020). Mediterranean overflow water in the North Atlantic and its multidecadal variability. *Tellus A: Dynamic Meteorology and Oceanography* 72 (1), 1–10.

Artale, V., Falcini, F., Marullo, S., Bensi, M., Kokoszka, F., Iudicone, D., et al. (2018). Linking mixing processes and climate variability to the heat content distribution of the Eastern Mediterranean abyss. *Sci. Rep.* 8 (1), 1–10. doi: 10.1038/s41598-018-29343-4

Artegiani, A., Azzolini, R., and Salusti, E. (1989). On the dense water in the Adriatic Sea. *Oceanologica Acta* 12 (2), 151–160.

Bensoussan, N., Chiggiato, J., Buongiorno Nardelli, B., Pisano, A., and Garrabou, J. (2019). *Insights on 2017 marine heat waves in the Mediterranean Sea*. Copernicus Marine Service Ocean State Report. (3), 101–108.

Berkes, F. (2017). *Sacred ecology* (New York: Routledge).

Berkes, F., and Turner, N. J. (2006). Knowledge, learning and the evolution of conservation practice for social-ecological system resilience. *Hum. Ecol.* 34, 479–494. doi: 10.1007/s10745-006-9008-2

Bernstein, L., Bosch, P., Canziani, O., Chen, Z., Christ, R., and Riahi, K. (2008). *IPCC, 2007: climate change 2007: synthesis report.*

Bessières, L., Rio, M. H., Dufau, C., Boone, C., and Pujol, M. I. (2013). Ocean state indicators from MyOcean altimeter products. *Ocean Sci.* 9 (3), 545–560. doi: 10.5194/os-9-545-2013

Béthoux, J. P., Gentili, B., and Tailliez, D. (1998). Warming and freshwater budget change in the Mediterranean since the 1940s, their possible relation to the greenhouse effect. *Geophysical Res. Lett.* 25 (7), 1023–1026. doi: 10.1029/98GL00724

Bianchi, C. N., and Morri, C. (2000). Marine biodiversity of the Mediterranean Sea: situation, problems and prospects for future research. *Mar. pollut. Bull.* 40 (5), 367–376. doi: 10.1016/S0025-326X(00)00027-8

Bindoff, N. L., Cheung, W. W. L., Kairo, J. G., Arístegui, J., Guinder, V. A., Hallberg, R., et al. (2019). IPCC special report on the ocean and cryosphere in a changing climate. *Intergovernmental Panel Climate Change*, 477–587.

Brondízio, E. S., Aumeeruddy-Thomas, Y., Bates, P., Carino, J., Fernández-Llamazares, Á., Ferrari, M. F., et al. (2021). Locally based, regionally manifested, and globally relevant: Indigenous and local knowledge, values, and practices for nature. *Annu. Rev. Environ. Res.* 46, 481–509.

Cabanes, C., Angel-Benavides, I., Buck, J., Coatanoan, C., Dobler, D., Herbert, G., et al. (2021). DMQC Cookbook for Core Argo parameters. doi: 10.13155/78994

Cardin, V., Bensi, M., and Pacciaroni, M. (2011). Variability of water mass properties in the last two decades in the South Adriatic Sea with emphasis on the period 2006–2009. *Continental Shelf Res.* 31 (9), 951–965. doi: 10.1016/j.csr.2011.03.002

Cardin, V., Wirth, A., Khosravi, M., and Gačić, M. (2020). South adriatic recipes: estimating the vertical mixing in the deep Pit. *Front. Mar. Sci.* 7, 565982. doi: 10.3389/fmars.2020.565982

Cheng, L., Abraham, J., Trenberth, K. E., Fasullo, J., Boyer, T., Mann, M. E., et al. (2023). Another year of record heat for the oceans. *Adv. Atmospheric Sci.*, 1–12. doi: 10.1007/s00376-023-2385-2

Church, J. A., and White, N. J. (2011). Sea-level rise from the late 19th to the early 21st century. *Surveys geophysics* 32 (4), 585–602. doi: 10.1007/s10712-011-9119-1

Civitarese, G., Gačić, M., Cardin, V., and Ibello, V. (2005). Winter convection continues in the warming Southern Adriatic. *Eos Trans. Am. Geophysical Union* 86 (45), 445–451. doi: 10.1029/2005EO450002

Civitarese, G., Gačić, M., Lipizer, M., and Eusebi Borzelli, G. L. (2010). On the impact of the Bimodal Oscillating System (BiOS) on the biogeochemistry and biology of the Adriatic and Ionian Seas (Eastern Mediterranean). *Biogeosciences* 7 (12), 3987–3997. doi: 10.5194/bg-7-3987-2010

Coll, M., Piroddi, C., Steenbeek, J., Kaschner, K., Ben Rais Lasram, F., Aguzzi, J., et al. (2010). The biodiversity of the Mediterranean Sea: estimates, patterns, and threats. *PLoS One* 5 (8), e11842. doi: 10.1371/journal.pone.0011842

Coma, R., Ribes, M., Serrano, E., Jiménez, E., Salat, J., and Pascual, J. (2009). Global warming-enhanced stratification and mass mortality events in the Mediterranean. *Proc. Natl. Acad. Sci.* 106 (15), 6176–6181. doi: 10.1073/pnas.0805801106

Conan, P., Testor, P., Estournel, C., d'Ortenzio, F., Pujo-Pay, M., and Durrieu de Madron, X. (2018). Preface to the Special Section: Dense water formations in the northwestern Mediterranean: From the physical forcings to the biogeochemical consequences. *J. Geophysical Research: Oceans* 123 (10), 6983–6995.

Criado-Aldeanueva, F., Vera, J. D. R., and García-Lafuente, J. (2008). Steric and mass-induced Mediterranean sea level trends from 14 years of altimetry data. *Global Planetary Change* 60 (3-4), 563–575. doi: 10.1016/j.gloplacha.2007.07.003

Darmaraki, S., Somot, S., Sevault, F., and Nabat, P. (2019b). Past variability of Mediterranean Sea marine heatwaves. *Geophysical Res. Lett.* 46 (16), 9813–9823. doi: 10.1029/2019GL082933

Darmaraki, S., Somot, S., Sevault, F., Nabat, P., Cabos Narvaez, W. D., Cavicchia, L., et al. (2019a). Future evolution of marine heatwaves in the Mediterranean Sea. *Climate Dynamics* 53, 1371–1392. doi: 10.1007/s00382-019-04661-z

Dayan, H., McAdam, R., Juza, M., Masina, S., and Speich, S. (2023). Marine heat waves in the Mediterranean Sea: An assessment from the surface to the subsurface to meet national needs. *Front. Mar. Sci.* 10, 1045138. doi: 10.3389/fmars.2023.1045138

de Pascual-Collar, Á., G Sotillo, M., Levier, B., Aznar, R., Lorente, P., Amo-Baladrón, A., et al. (2019). Regional circulation patterns of Mediterranean Outflow Water near the Iberian and African continental slopes. *Ocean Sci.* 15 (3), 565–582. doi: 10.5194/os-15-565-2019

Durrieu de Madron, X., Houpert, L., Puig, P., Sanchez-Vidal, A., Testor, P., Bosse, A., et al. (2013). Interaction of dense shelf water cascading and open-sea convection in the northwestern Mediterranean during winter 2012. *Geophysical Res. Lett.* 40 (7), 1379–1385. doi: 10.1002/grl.50331

Ehlers, P. (2016). Blue growth and ocean governance—how to balance the use and the protection of the seas. *WMU J. Maritime Affairs* 15 (2), 187–203. doi: 10.1007/s13437-016-0104-x

Estournel, C., Testor, P., Taupier-Letage, I., Bouin, M. N., Coppola, L., Durand, P., et al. (2016). HyMeX-SOP2: The field campaign dedicated to dense water formation in the northwestern Mediterranean. *Oceanography* 29 (4), 196–206. doi: 10.5670/oceanog.2016.94

Fragkopoulou, E., Costello, M. J., Gupta, A. S., Wernberg, T., Araújo, M. B., Serrão, E. A., et al. (2023). Marine biodiversity exposed to prolonged and intense subsurface heatwaves. *ON Mar. Sci.* 84. doi: 10.1038/s41558-023-01790-6

Frölicher, T. L., Fischer, E. M., and Gruber, N. (2018). Marine heatwaves under global warming. *Nature* 560 (7718), 360–364.

Gačić, M., Borzelli, G. E., Civitarese, G., Cardin, V., and Yari, S. (2010). Can internal processes sustain reversals of the ocean upper circulation? The Ionian Sea example. *Geophysical Res. Lett.* 37 (9).

Gačić, M., Civitarese, G., Eusebi Borzelli, G. L., Kovačević, V., Poulain, P. M., Theocharis, A., et al. (2011). On the relationship between the decadal oscillations of the

northern Ionian Sea and the salinity distributions in the eastern Mediterranean. *J. Geophysical Research: Oceans* 116 (C12).

Gačić, M., Lascaratos, A., Manca, B. B., and Mantziafou, A. (2001). "Adriatic deep water and interaction with the Eastern Mediterranean Sea," in *Physical oceanography of the Adriatic Sea: Past, present and future* (Dordrecht: Springer Netherlands), 111–142.

Gačić, M., Schroeder, K., Civitarese, G., Cosoli, S., Vetrano, A., and Eusebi Borzelli, G. L. (2013). Salinity in the Sicily Channel corroborates the role of the Adriatic–Ionian Bimodal Oscillating System (BiOS) in shaping the decadal variability of the Mediterranean overturning circulation. *Ocean Sci.* 9 (1), 83–90.

Gačić, M., Ursella, L., Kovačević, V., Menna, M., Malačič, V., Bensi, M., et al. (2021). Impact of dense-water flow over a sloping bottom on open-sea circulation: laboratory experiments and an Ionian Sea (Mediterranean) example. *Ocean Sci.* 17 (4), 975–996.

Galassi, G., and Spada, G. (2014). Sea-level rise in the Mediterranean Sea by 2050: Roles of terrestrial ice melt, steric effects and glacial isostatic adjustment. *Global Planetary Change* 123, 55–66. doi: 10.1016/j.gloplacha.2014.10.007

Garrabou, J., Gómez-Gras, D., Medrano, A., Cerrano, C., Ponti, M., Schlegel, R., et al. (2022). Marine heatwaves drive recurrent mass mortalities in the Mediterranean Sea. *Global Change Biol.* 28 (19), 5708–5725. doi: 10.1111/gcb.16301

Giorgi, F. (2006). Climate change hot-spots. *Geophysical Res. Lett.* 33 (8). doi: 10.1029/2006GL025734

Giorgi, F., and Lionello, P. (2008). Climate change projections for the Mediterranean region. *Global planetary Change* 63 (2-3), 90–104. doi: 10.1016/j.gloplacha.2007.09.005

Gonzalez-Santana, A., Oosterbaan, M., Clavelle, T., Maze, G., Notarstefano, G., Poffa, N., et al. (2023). Analysis of the global shipping traffic for the feasibility of a structural recovery program of Argo floats. *Front. Mar. Sci.* 10. doi: 10.3389/fmars.2023.1161580

Grignon, L., Smeed, D. A., Bryden, H. L., and Schroeder, K. (2010). Importance of the variability of hydrographic preconditioning for deep convection in the Gulf of Lion, NW Mediterranean. *Ocean Sci.* 6 (2), 573–586. doi: 10.5194/os-6-573-2010

Hamdeno, M., and Alvera-Azcarate, A. (2023). Marine heatwaves characteristics in the Mediterranean Sea: Case study the 2019 heatwave events. *Front. Mar. Sci.* 10, 1093760. doi: 10.3389/fmars.2023.1093760

Hansen, J., Sato, M., Kharecha, P., and Von Schuckmann, K. (2011). Earth's energy imbalance and implications. *Atmospheric Chem. Phys.* 11 (24), 13421–13449. doi: 10.5194/acp-11-13421-2011

Hansen, J., Sato, M. K. I., Ruedy, R., Nazarenko, L., Lacis, A., Schmidt, G. A., et al. (2005). Efficacy of climate forcings. *J. geophysical research: atmospheres* 110 (D18).

Ibrahim, O., Mohamed, B., and Nagy, H. (2021). Spatial variability and trends of marine heat waves in the eastern mediterranean sea over 39 years. *J. Mar. Sci. Eng.* 9 (6), 643. doi: 10.3390/jmse9060643

Iona, A., Theodorou, A., Sofianos, S., Watelet, S., Troupin, C., and Beckers, J. M. (2018). Mediterranean Sea climatic indices: monitoring long-term variability and climate changes. *Earth System Sci. Data* 10 (4), 1829–1842. doi: 10.5194/essd-10-1829-2018

Janeković, I., Mihanović, H., Vilibić, I., and Tudor, M. (2014). Extreme cooling and dense water formation estimates in open and coastal regions of the Adriatic Sea during the winter of 2012. *J. Geophysical Research: Oceans* 119 (5), 3200–3218. doi: 10.1002/2014JC009865

Josey, S. A., and Schroeder, K. (2023). Declining winter heat loss threatens continuing ocean convection at a Mediterranean dense water formation site. *Environ. Res. Lett.* 18 (2), 024005.

Juza, M., and Tintoré, J. (2021). Multivariate Sub-regional ocean indicators in the Mediterranean Sea: From event detection to climate change estimations. *Front. Mar. Sci.* 8, 610589.

Juza, M., Fernández-Mora, À., and Tintoré, J. (2022). Sub-Regional marine heat waves in the Mediterranean Sea from observations: Long-term surface changes, Sub-surface and coastal responses. *Front. Mar. Sci.* 9, 785771. doi: 10.3389/fmars.2022.785771

Kealiikanakaoleohaililani, K., and Giardina, C. P. (2016). Embracing the sacred: an indigenous framework for tomorrow's sustainability science. *Sustainability Sci.* 11, 57–67. doi: 10.1007/s11625-015-0343-3

Kimmerer, R. W. (2012). Searching for synergy: Integrating traditional and scientific ecological knowledge in environmental science education. *J. Environ. Stud. Sci.* 2, 317–323. doi: 10.1007/s13412-012-0091-y

Kirtman, B., Power, S. B., Adedoyin, A. J., Boer, G. J., Bojariu, R., Camilloni, I., et al. (2013). Near-term Climate Change: Projections and Predictability. In: *Climate Change 2013: The Physical Science Basis. Contribution of Working Group I to the Fifth Assessment Report of the Intergovernmental Panel on Climate Change* eds. T. F. Stocker, D. Qin, G.-K. Plattner, M. Tignor, S. K. Allen, J. Boschung, et al (Cambridge, United Kingdom and New York, NY, USA: Cambridge University Press).

Klein, B., Roether, W., Civitarese, G., Gacic, M., Manca, B. B., and d'Alcala, M. R. (2000). Is the Adriatic returning to dominate the production of Eastern Mediterranean Deep Water? *Geophysical Res. Lett.* 27 (20), 3377–3380.

Knutti, R., and Rugenstein, M. A. (2015). Feedbacks, climate sensitivity and the limits of linear models. *Philos. Trans. R. Soc. A: Mathematical Phys. Eng. Sci.* 373 (2054), 20150146.

Kubin, E., Poulain, P. M., Mauri, E., Menna, M., and Notarstefano, G. (2019). Levantine intermediate and Levantine deep water formation: An Argo float study from 2001 to 2017. *Water* 11 (9), 1781. doi: 10.3390/w11091781

Lambeck, K., and Bard, E. (2000). Sea-level change along the French Mediterranean coast for the past 30 000 years. *Earth Planetary Sci. Lett.* 175 (3-4), 203–222. doi: 10.1016/S0012-821X(99)00289-7

Lascaratos, A., Roether, W., Nittis, K., and Klein, B. (1999). Recent changes in deep water formation and spreading in the eastern Mediterranean Sea: a review. *Prog. oceanography* 44 (1-3), 5–36. doi: 10.1016/S0079-6611(99)00019-1

Levitus, S., Antonov, J., and Boyer, T. (2005). Warming of the world ocean 1955–2003. *Geophysical Res. Lett.* 32 (2). doi: 10.1029/2004GL021592

Levitus, S., Antonov, J. I., Boyer, T. P., Baranova, O. K., Garcia, H. E., Locarnini, R. A., et al. (2012). World ocean heat content and thermosteric sea level change (0–2000 m), 1955–2010. *Geophysical Res. Lett.* 39 (10). doi: 10.1029/2012GL051106

Lionello, P., and Scarascia, L. (2018). The relation between climate change in the Mediterranean region and global warming. *Regional Environ. Change* 18 (5), 1481–1493. doi: 10.1007/s10113-018-1290-1

Lo Bue, N., Artale, V., and Schroeder, K. (2021). Impact of deep oceanic processes on circulation and climate variability: examples from the Mediterranean sea and the global ocean. *Front. Mar. Sci.*, 1874.

Malanotte-Rizzoli, P., Manca, B. B., Marullo, S., Ribera d'Alcala', M., Roether, W., Theocharis, A., et al. (2003). The Levantine Intermediate Water Experiment (LIWEX) Group: Levantine basin - A laboratory for multiple water mass formation processes. *J. Geophysical Research: Oceans* 108 (C9).

Manca, B. B., Kovaĉević, V., Gaĉić, M., and Viezzoli, D. (2002). Dense water formation in the Southern Adriatic Sea and spreading into the Ionian Sea in the period 1997–1999. *J. Mar. Syst.* 33, 133–154. doi: 10.1016/S0924-7963(02)00056-8

Marcos, M., and Tsimplis, M. N. (2007). Variations of the seasonal sea level cycle in southern Europe. *J. Geophysical Research: Oceans* 112 (C12).

Margirier, F., Testor, P., Heslop, E., Mallil, K., Bosse, A., Houpert, L., et al. (2020). Abrupt warming and salinification of intermediate waters interplays with decline of deep convection in the Northwestern Mediterranean Sea. *Sci. Rep.* 10 (1), 20923.

Menna, M., Gačić, M., Martellucci, R., Notarstefano, G., Fedele, G., Mauri, E., et al. (2022). Climatic, decadal, and interannual variability in the upper layer of the Mediterranean Sea using remotely sensed and *in-situ* data. *Remote Sens.* 14 (6), 1322. doi: 10.3390/rs14061322

Menna, M., Suarez, N. R., Civitarese, G., Gačić, M., Rubino, A., and Poulain, P. M. (2019). Decadal variations of circulation in the Central Mediterranean and its interactions with mesoscale gyres. *Deep Sea Res. Part II: Topical Stud. Oceanography* 164, 14–24.

Mieruch, S., Noël, S., Bovensmann, H., and Burrows, J. P. (2008). Analysis of global water vapour trends from satellite measurements in the visible spectral range. *Atmospheric Chem. Phys.* 8 (3), 491–504. doi: 10.5194/acp-8-491-2008

Mihanović, H., Vilibić, I., Šepić, J., Matić, F., Ljubešić, Z., Mauri, E., et al. (2021). Observation, preconditioning and recurrence of exceptionally high salinities in the Adriatic Sea. *Front. Mar. Sci.* 8, 672210. doi: 10.3389/fmars.2021.672210

Millero, F. J., Perron, G., and Desnoyers, J. E. (1973). Heat capacity of seawater solutions from 5 to 35 C and 0.5 to 22‰ chlorinity. *J. Geophysical Res.* 78 (21), 4499–4507. doi: 10.1029/JC078i021p04499

Millot, C., Candela, J., Fuda, J. L., and Tber, Y. (2006). Large warming and salinification of the Mediterranean outflow due to changes in its composition. *Deep Sea Res. Part I: Oceanographic Res. Papers* 53 (4), 656–666. doi: 10.1016/j.dsr.2005.12.017

Minerbi, L. (1999). Indigenous management models and protection of the ahupua A'. *Soc Process Hawai 'i* 39, 208–225.

Naranjo, C., Sammartino, S., García-Lafuente, J., Bellanco, M. J., and Taupier-Letage, I. (2015). Mediterranean waters along and across the Strait of Gibraltar, characterization and zonal modification. *Deep Sea Res. Part I: Oceanographic Res. Papers* 105, 41–52.

Nittis, K., Lascaratos, A., and Theocharis, A. (2003). Dense water formation in the Aegean Sea: Numerical simulations during the Eastern Mediterranean Transient. *J. Geophysical Research: Oceans* 108 (C9).

Oliver, E. C., Benthuysen, J. A., Darmaraki, S., Donat, M. G., Hobday, A. J., Holbrook, N. J., et al. (2021). Marine heatwaves. *Annu. Rev. Mar. Sci.* 13, 313–342. doi: 10.1146/annurev-marine-032720-095144

Ozer, T., Gertman, I., Kress, N., Silverman, J., and Herut, B. (2017). Interannual thermohaline, (1979–2014) and nutrient, (2002–2014) dynamics in the Levantine surface and intermediate water masses, SE Mediterranean Sea. *Global Planetary Change* 151, 60–67. doi: 10.1016/j.gloplacha.2016.04.001

Pinardi, N., Cessi, P., Borile, F., and Wolfe, C. L. (2019). The Mediterranean sea overturning circulation. *J. Phys. Oceanography* 49 (7), 1699–1721. doi: 10.1175/JPO-D-18-0254.1

Pisano, A., Marullo, S., Artale, V., Falcini, F., Yang, C., Leonelli, F. E., et al. (2020). New evidence of mediterranean climate change and variability from sea surface temperature observations. *Remote Sens.* 12 (1), 132. doi: 10.3390/rs12010132

Placenti, F., Torri, M., Pessini, F., Patti, B., Tancredi, V., Cuttitta, A., et al. (2022). Hydrological and biogeochemical patterns in the Sicily channel: New insights from the last decade, (2010-2020). *Front. Mar. Sci.* 9, 733540. doi: 10.3389/fmars.2022.733540

Potter, R. A., and Béthoux, M. S. (2004). On the warming and salinification of the Mediterranean outflow waters in the North Atlantic. *Geophysical Res. Lett.* 31 (1). doi: 10.1029/2003GL018161

Poulain, P. M., Barbanti, R., Font, J., Cruzado, A., Millot, C., Gertman, I., et al. (2007). MedArgo: a drifting profiler program in the Mediterranean Sea. *Ocean Sci.* 3 (3), 379–395. doi: 10.5194/os-3-379-2007

Rahmstorf, S. (1998). Influence of Mediterranean outflow on climate. *Eos Trans. Am. Geophysical Union* 79 (24), 281–282. doi: 10.1029/98EO00208

Reale, M., Salon, S., Crise, A., Farneti, R., Mosetti, R., and Sannino, G. (2017). Unexpected covariant behavior of the Aegean and Ionian Seas in the period 1987–2008 by means of a nondimensional sea surface height index. *J. Geophysical Research: Oceans* 122 (10), 8020–8033. doi: 10.1002/2017JC012983

Reed, M. G. (2019). The contributions of UNESCO Man and Biosphere Programme and biosphere reserves to the practice of sustainability science. *Sustainability Sci.* 14 (3), 809–821. doi: 10.1007/s11625-018-0603-0

Rhein, M., Rintoul, S. R., Aoki, S., Campos, E., Chambers, D., Feely, R. A., et al. (2013). Observations: ocean in climate change 2013: the physical science basis. Contribution of working group I to the fifth assessment report of the intergovernmental panel on climate change. *Fifth Assess. Rep. Intergovernmental Panel Climate Change*, 255–316.

Roether, W., Klein, B., Manca, B. B., Theocharis, A., and Kioroglou, S. (2007). Transient Eastern Mediterranean deep waters in response to the massive dense-water output of the Aegean Sea in the 1990s. *Prog. Oceanography* 74 (4), 540–571. doi: 10.1016/j.pocean.2007.03.001

Rubino, A., Gačić, M., Bensi, M., Kovačević, V., Malačič, V., Menna, M., et al. (2020). Experimental evidence of long-term oceanic circulation reversals without wind influence in the North Ionian Sea. *Sci. Rep.* 10 (1), 1905.

Rubino, A., Romanenkov, D., Zanchettin, D., Cardin, V., Hainbucher, D., Bensi, M., et al. (2012). On the descent of dense water on a complex canyon system in the southern Adriatic basin. *Continental Shelf Res.* 44, 20–29. doi: 10.1016/j.csr.2010.11.009

Schroeder, K., Chiggiato, J., Josey, S. A., Borghini, M., Aracri, S., and Sparnocchia, S. (2017). Rapid response to climate change in a marginal sea. *Sci. Rep.* 7 (1), 1–7. doi: 10.1038/s41598-017-04455-5

Smith, K. E., Burrows, M. T., Hobday, A. J., King, N. G., Moore, P. J., Sen Gupta, A., et al. (2022). Biological impacts of marine heatwaves. *Annu. Rev. Mar. Sci.* 15.

Tamburini, C., Canals, M., Durrieu de Madron, X., Houpert, L., and Lefevre, D. (2013). Deep-Sea bioluminescence blooms after dense water formation at the ocean surface. *PLoS ONE* 8 (7), e67523. doi: 10.1371/journal.pone.0067523

Theocharis, A., and Georgopoulos, D. (1993). Dense water formation over the Samothraki and Limnos Plateaux in the north Aegean Sea (eastern Mediterranean Sea). *Continental Shelf Res.* 13 (8-9), 919–939. doi: 10.1016/0278-4343(93)90017-R

Theocharis, A., Krokos, G., Velaoras, D., and Korres, G. (2014). An internal mechanism driving the alternation of the Eastern Mediterranean dense/deep water sources. *Mediterr. Sea: Temporal variability spatial patterns*, 113–137. doi: 10.1002/9781118847572.ch8

Trenberth, K. E., Fasullo, J. T., and Balmaseda, M. A. (2014). Earth's energy imbalance. *J. Climate* 27 (9), 3129–3144. doi: 10.1175/JCLI-D-13-00294.1

Trenberth, K. E., Fasullo, J. T., and Kiehl, J. (2009). Earth's global energy budget. *Bull. Am. Meteorological Soc.* 90 (3), 311–324. doi: 10.1175/2008BAMS2634.1

Trenberth, K. E., and Stepaniak, D. P. (2004). The flow of energy through the Earth's climate system. *Q. J. R. Meteorological Soc.* 130 (603), 2677–2701. doi: 10.1256/qj.04.83

Tsimplis, M., Marcos, M., Somot, S., and Barnier, B. (2008). Sea level forcing in the Mediterranean Sea between 1960 and 2000. *Global Planetary Change* 63 (4), 325–332. doi: 10.1016/j.gloplacha.2008.07.004

Vargas-Yáñez, M., García, M. J., Salat, J., García-Martínez, M. C., Pascual, J., and Moya, F. (2008). Warming trends and decadal variability in the Western Mediterranean shelf. *Global Planetary Change* 63 (2-3), 177–184. doi: 10.1016/j.gloplacha.2007.09.001

Vargas-Yáñez, M., García-Martínez, M. C., Moya, F., Balbín, R., López-Jurado, J. L., Serra, M., et al. (2017). Updating temperature and salinity mean values and trends in the Western Mediterranean: The RADMED project. *Prog. Oceanography* 157, 27–46. doi: 10.1016/j.pocean.2017.09.004

Velaoras, D., and Lascaratos, A. (2010). North–Central Aegean Sea surface and intermediate water masses and their role in triggering the Eastern Mediterranean Transient. *J. Mar. Syst.* 83 (1-2), 58–66. doi: 10.1016/j.jmarsys.2010.07.001

Vilibić, I., and Supić, N. (2005). Dense water generation on a shelf: the case of the Adriatic Sea. *Ocean Dynamics* 55 (5), 403–415. doi: 10.1007/s10236-005-0030-5

Von Schuckmann, K., Cheng, L., Palmer, M. D., Hansen, J., Tassone, C., Aich, V., et al. (2020). Heat stored in the Earth system: where does the energy go? *Earth System Sci. Data* 12 (3), 2013–2041.

Von Schuckmann, K., Gaillard, F., and Le Traon, P. Y. (2009). Global hydrographic variability patterns during 2003–2008. *J. Geophysical Research: Oceans* 114 (C9).

Von Schuckmann, K., and Le Traon, P. Y. (2011). How well can we derive Global Ocean Indicators from Argo data? *Ocean Sci.* 7 (6), 783–791.

Von Schuckmann, K., Le Traon, P. Y., Smith, N., Pascual, A., Brasseur, P., Fennel, K., et al. (2018). Copernicus marine service ocean state report. *J. Operational Oceanography* 11 (sup1), S1–S142. doi: 10.1080/1755876X.2018.1489208

von Schuckmann, K., Le Traon, P. Y., Smith, N., Pascual, A., Djavidnia, S., Gattuso, J. P., et al. (2019). Copernicus marine service ocean state report, issue 3. *J. Operational Oceanography* 12 (sup1), S1–S123. doi: 10.1080/1755876X.2019.1633075

von Schuckmann, K., Palmer, M. D., Trenberth, K. E., Cazenave, A., Chambers, D., Champollion, N., et al. (2016). An imperative to monitor Earth's energy imbalance. *Nat. Climate Change* 6 (2), 138–144. doi: 10.1038/nclimate2876

Waldman, R., Brüggemann, N., Bosse, A., Spall, M., Somot, S., and Sevault, F. (2018). Overturning the Mediterranean thermohaline circulation. *Geophysical Res. Lett.* 45 (16), 8407–8415. doi: 10.1029/2018GL078502

Weatherhead, E. C., Reinsel, G. C., Tiao, G. C., Meng, X. L., Choi, D., Cheang, W. K., et al. (1998). Factors affecting the detection of trends: Statistical considerations and applications to environmental data. *J. Geophysical Research: Atmospheres* 103 (D14), 17149–17161.

Witte, F. X. P., and Xué, F. (2018). *Living the Law of Origin: The Cosmological, Ontological, Epistemological, and Ecological Framework of Kogi Environmental Politics*. Doctoral dissertation. (Cambridge, UK: University of Cambridge).

Wong, A. P., Wijffels, S. E., Riser, S. C., Pouliquen, S., Hosoda, S., Roemmich, D., et al. (2020). Argo data 1999–2019: Two million temperature-salinity profiles and subsurface velocity observations from a global array of profiling floats. *Front. Mar. Sci.* 7, 700. doi: 10.3389/fmars.2020.00700